

## Thin SnO<sub>2</sub> nanowires produced with a varying oxygen gas flow ratio and their structural, Raman, and electronic properties

Han Gil Na, Dong Sub Kwak, Yong Jung Kwon, Fan Xia, Won Il Park and Hyoun Woo Kim\*

Division of Materials Science and Engineering, Hanyang University, Seoul 133-791, Republic of Korea

We have investigated the effects of the oxygen gas flow ratio in a synthesis process, ultimately producing thin (~40 nm in diameter) SnO<sub>2</sub> nanowires. Scanning electron microscopy revealed that the oxygen partial pressure affected the diameter as well as the length of the nanowires. An X-ray diffraction investigation suggested that the grain size of the SnO<sub>2</sub> phase was slightly increased with a decrease in the oxygen partial pressure. Lattice-resolved transmission electron microscopy (TEM) images, selected area electron diffraction, and micro-Raman spectroscopy coincidentally showed that the as-synthesized nanowires comprised a tetragonal SnO<sub>2</sub> phase. Based on the analysis by fabricating field effect transistors, we found that the transport properties of SnO<sub>2</sub> nanowires exhibited an n-type semiconductor characteristic.

**Key words:** SnO<sub>2</sub>, Nanowires, Field effect transistors (FETs), Raman spectroscopy

### Introduction

Since nanostructured materials have specific physical and chemical properties, attention has been focused on the research of these materials over the past several years [1-14]. SnO<sub>2</sub> nanowires have recently been intensively studied for possible applications such as in field emission [15], dye-sensitized solar cells [16], gas sensors [17], photodetectors [18], electrocatalysts [19], fully-transparent thin-film transistors [20], nanoengineered chemiresistors [21], and lithium-ion batteries [22], etc.

Because their special importance, SnO<sub>2</sub> nanowires have been fabricated with a variety of techniques, including a hydrothermal method [23], by chemical vapor deposition [24], a polyol method [25], by direct sublimation of SnO<sub>2</sub> nanoparticles [26], by carbothermal reduction of SnO [27], and oxidizing SnO nanoparticles [28].

In the present paper, we have used a relatively simple and controllable technique, in which Sn powders were heated in an O<sub>2</sub>/Ar ambient. Herein, we have varied the O<sub>2</sub> partial pressure, investigating the changes in the nanowire properties. In the field of nanostructures including nanowires, a study of changes induced by varying the process parameters has rarely been carried out and thus this report will become a cornerstone. In addition, we have fabricated field effect transistors (FETs) with the nanowires prepared, evaluating the electronic properties of the SnO<sub>2</sub> nanowires.

### Experimental

The SnO<sub>2</sub> nanowires were fabricated in a tube furnace, by heating the Sn powders at 900°C for 1 minute. An Au (approximate thickness=3 nm)-coated Si substrate has been employed. During the experiment, a mixture of Ar and O<sub>2</sub> gases was flowed. In order to investigate the effect of O<sub>2</sub> gas injection, the percentages of the O<sub>2</sub> and the Ar partial pressures, were set to 0 and 100%, 0.5 and 99.5%, 1.0 and 99.0%, and 2.7 and 97.3%.

We have analyzed samples by means of X-ray diffraction (XRD) (Philips X'pert MRD diffractometer with CuK<sub>α</sub>1 radiation), scanning electron microscopy (SEM) (Hitachi, S-4200), and transmission electron microscopy (TEM) (Philips, CM-200). Micro-Raman spectra were acquired using the 633 nm line of an He-Ne laser. Raman spectra were recorded at room temperature in an air ambient using a Renishaw Raman spectromicroscope at Korean Basic Science Institute (KBSI).

To measure the electronic properties, field-effect transistors (FETs) were fabricated based on the as-synthesized SnO<sub>2</sub> nanowires [29]. The as-synthesized SnO<sub>2</sub> nanowires were transformed to the SiO<sub>2</sub>/Si, in which the heavily doped p-type Si substrate and a 200-nm-thick SiO<sub>2</sub> layer were used as a back gate electrode and an insulating gate dielectric layer, respectively. The electrodes were patterned by photolithography, with Ti/Au (10/50 nm) electrodes being subsequently deposited. The electrical characteristics of the SnO<sub>2</sub> nanowire FETs were measured at room temperature under ambient conditions using a semiconductor parameter analyzer (HP4145).

\*Corresponding author:  
Tel : +82-10-8428-0883  
Fax: +82-2-2220-0389  
E-mail: hyounwoo@hanyang.ac.kr

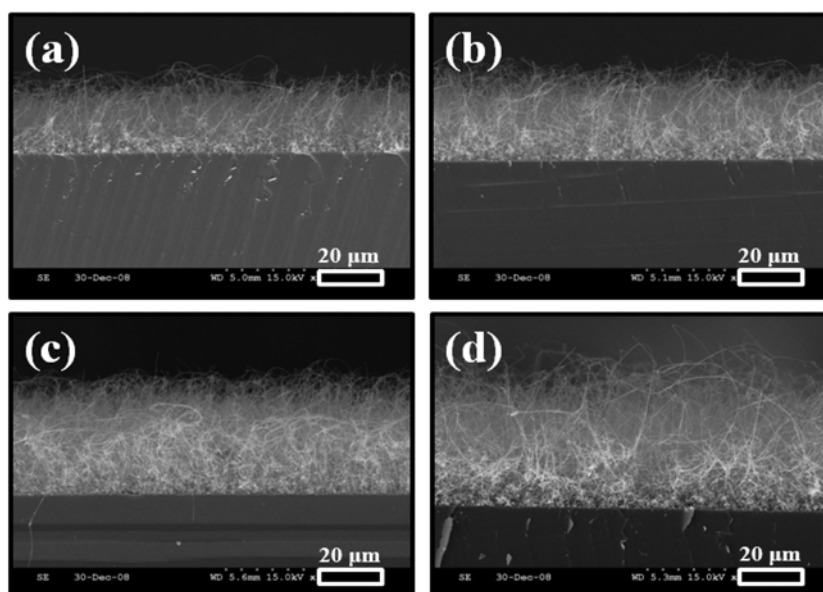


Fig. 1. Side-view SEM images of the products with  $O_2$  partial pressures of (a) 0, (b) 0.5, (c) 1.0, and (d) 2.7%.

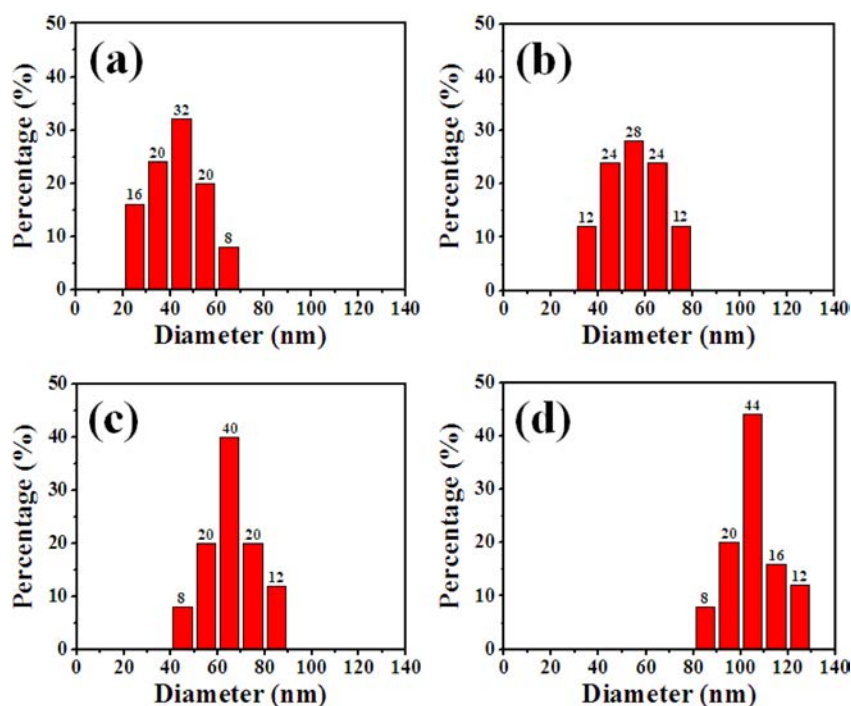


Fig. 2. Diameter distributions of the nanowires produced with  $O_2$  partial pressures of (a) 0, (b) 0.5, (c) 1.0, and (d) 2.7%.

## Results and discussion

Figs. 1a, 1b, 1c, and 1d show the side-view SEM images of the products, in which the  $O_2$  partial pressure percentages during the synthetic process were 0 (sample A), 0.5 (sample B), 1.0 (sample C), and 2.7% (sample D), respectively. The overall morphology of the products is film-like, which consist of bundles of one-dimensional (1D) nanowires. The film thicknesses of the products increased with an increase in the  $O_2$  partial pressure, in which the thicknesses of the

products with the  $O_2$  partial pressure of 0, 0.5, 1.0, and 2.7%, respectively, are 33, 44, 54, and 64  $\mu\text{m}$ . Accordingly, we suggest that the  $O_2$  partial pressure played a crucial role in growing nanowires. We surmise that the amount of Sn powers is relatively abundant, reducing the  $O_2$  partial pressure resulted in lower growth of nanowires. In the present case, the supply of  $O_2$  vapor can be a rate-determining step.

The diameter distributions of samples A, B, C, and D, are shown in Figs. 2a, 2b, 2c, and 2d, respectively. The maxima of the diameter distributions occur in a

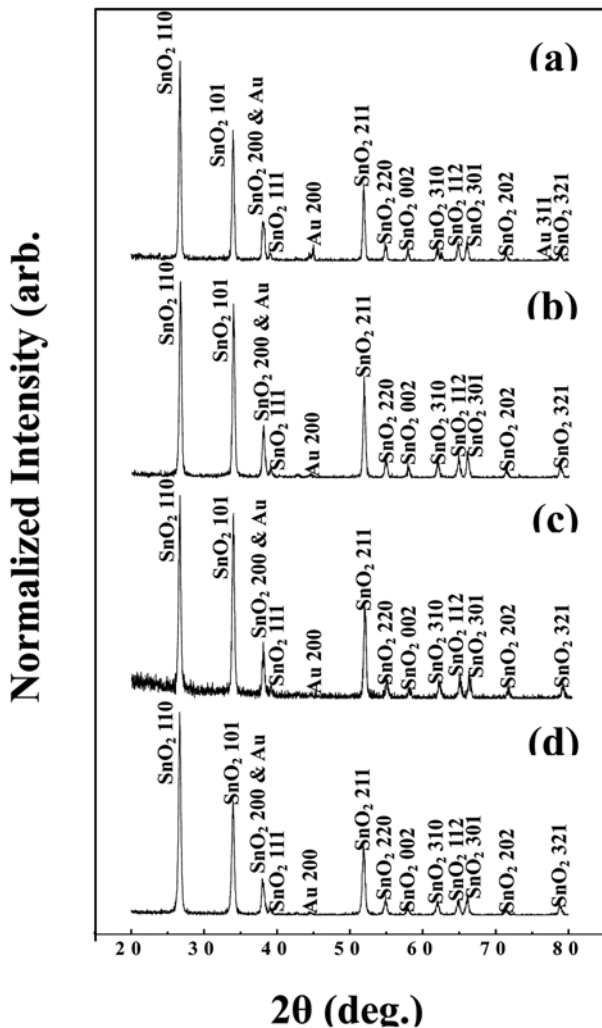


Fig. 3. (a) XRD patterns of the products with the O<sub>2</sub> partial pressures of (a) 0, (b) 0.5, (c) 1.0, and (d) 2.7%.

range of 40–50 nm, 50–60 nm, 60–70 nm, and 100–110 nm for samples A, B, C, and D, respectively. Based on Fig. 2, the average diameters of samples A, B, C, and D, were calculated to be about 40, 55, 66, and 105 nm, respectively. Accordingly, we reveal that the nanowire diameter was increased with an increase in the O<sub>2</sub> partial pressure during the synthesis process. We surmise that the growth of the 1D structure is an equilibrium process. In this case, with more supply of O<sub>2</sub> gas facilitating a more rapid reaction, the adsorbent on the nanowire surface does not easily migrate to the tip, which is an energetically-favored site at equilibrium. Accordingly, radial growth as well as axial growth may occur during the synthesis process, contributing to the thickening of the nanowires.

Figs. 3a, 3b, 3c, and 3d show XRD patterns of sample A, sample B, sample C, and sample D, respectively, indicating that the as-synthesized products are well-crystallized. Apart from a very weak peak of a cubic Au phase (JCPDS card: No. 04-0783), the sharp XRD peak could be well-indexed to the tetragonal

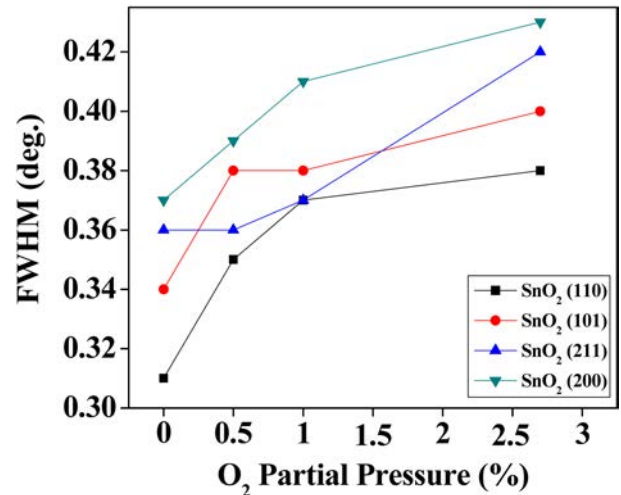


Fig. 4. Variation of the FWHM values for the (a) (110), (b) (101), (c) (211), and (d) (200) XRD peaks with varying the O<sub>2</sub> partial pressure during the synthesis process.

rutile structure of SnO<sub>2</sub> with lattice constants  $a=4.738$  Å and  $c=3.187$  Å (JCPDS File No. 41-1445). Since no prominent peaks from impurities were observed, the XRD spectra indicate that the products are of high purity.

Close examination revealed that the peak positions of the SnO<sub>2</sub>-related peaks are invariant, implying that the lattice constants of SnO<sub>2</sub> nanowires were fixed and did not depend on the process conditions. However, by investigating the widths of the main SnO<sub>2</sub>-related XRD peaks, we observed that the full-width-at-half-maximum (FWHM) values of the recognizable peaks, such as (110), (101), (211), and (200) reflections tended to increase with an increase in the O<sub>2</sub> partial pressure during the synthesis process (Fig. 4). Since XRD theory indicates that the grain size determined by XRD is inversely proportional to the FWHM value [30], we expect that the XRD grain size is increased with a decrease in the O<sub>2</sub> partial pressure during the synthesis process. This observation can be explained with respect to the SEM images and analysis (Figs. 1 and 2). In the process with a low O<sub>2</sub> partial pressure, a sufficiently slow process will contribute to the growth of larger grains. On the other hand, in the process with a high O<sub>2</sub> partial pressure, the relatively rapid process enables the nucleation of new grains on the side of nanowires. Accordingly, the growth of a single grain is a little suppressed, favoring the growth of many small grains.

Fig. 5a shows a low-magnification TEM image of a nanowire (sample A), with a diameter of about 39 nm. The nanowire exhibits a straight-line morphology with a growth direction along the  $\langle 001 \rangle$  axes. Fig. 5b shows a corresponding [010] zone axis selected area electron diffraction (SAED) pattern from the single nanowire, which indicates that the as-prepared SnO<sub>2</sub> nanowire is

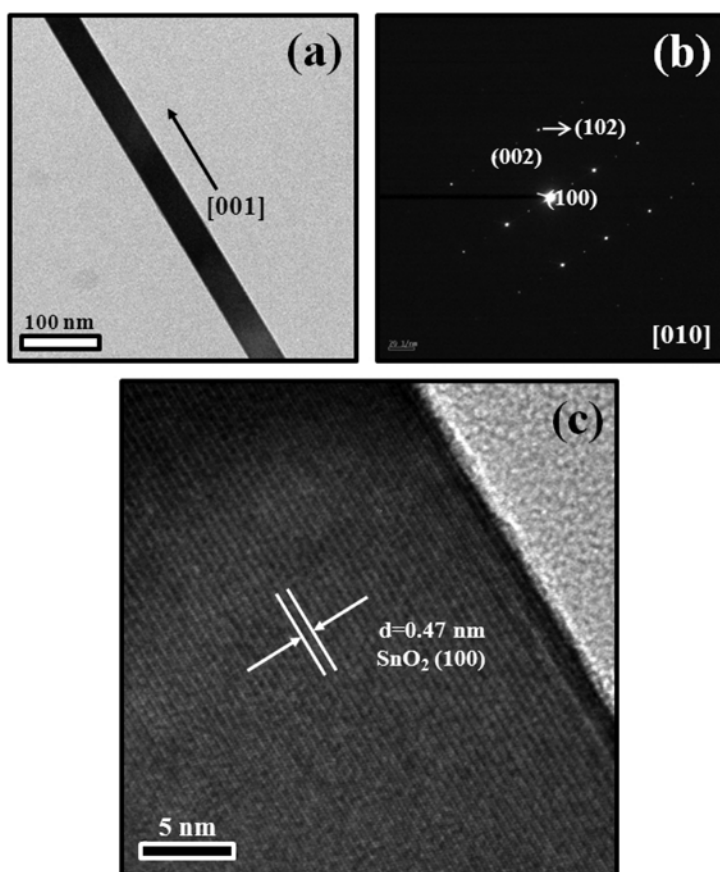


Fig. 5. (a) TEM image of a SnO<sub>2</sub> nanowire produced without O<sub>2</sub> flow. (b) Corresponding SAED pattern image. (c) Lattice-resolved TEM image.

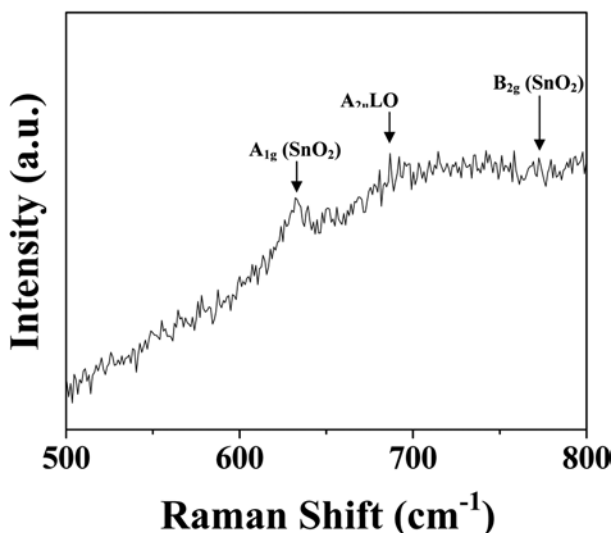


Fig. 6. Room-temperature Raman spectrum of typical SnO<sub>2</sub> nanowires.

single crystalline. Fig. 5c shows a high-resolution TEM image of a nanowire, in which the fringe spacing of 0.47 nm corresponds to the interplanar separation between the {100} planes.

Fig. 6 shows the room-temperature Raman spectrum of typical SnO<sub>2</sub> nanowires. Two fundamental Raman

peaks at 632 and 774 cm<sup>-1</sup>, corresponding to the A<sub>1g</sub> and B<sub>2g</sub> vibration modes, respectively, are observed, in good agreement with those for the rutile SnO<sub>2</sub> [31]. In addition, a weak Raman peak at 690-700 cm<sup>-1</sup> corresponds to the IR active A<sub>2u</sub>LO mode [32].

Fig. 7 shows a family of current-voltage (I-V) curves of a typical SnO<sub>2</sub> nanowire device under different gate biases (V<sub>g</sub>). Five curves at V<sub>g</sub> = -10 V, -5 V, 0 V, 5 V, and 10 V are displayed in this figure. The inset displays an I-V<sub>g</sub> plot of the device with the drain-source bias V<sub>d</sub> = -10 V, and a threshold gate voltage (V<sub>th</sub>) can be determined to be in the range of -1 to 0 V. It exhibits a typical curve, in which the I<sub>d</sub> decreases with a decrease in the V<sub>g</sub> at a fixed source-drain voltage (V<sub>d</sub>). Accordingly, the device shows a strong gate dependence, with the source-drain current (I<sub>d</sub>) increases with an increase in the V<sub>g</sub>, which is the typical behavior of an n-channel FET. It is noteworthy that the nanowires have never been intentionally doped. The possible reason for their being an n-type material might be due to oxygen vacancies and extra tin interstitial atoms in the lattice.

## Conclusions

In summary, we have varied the O<sub>2</sub> partial pressure,

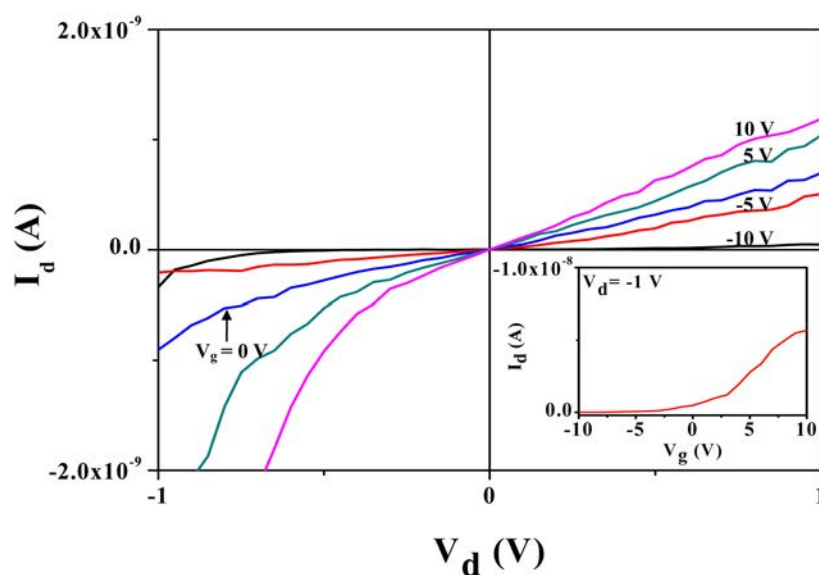


Fig. 7. Gate-dependent  $I_d$ - $V_d$  curves recorded at room temperature from FETs with SnO<sub>2</sub> nanowires (Inset:  $I_d$ - $V_g$  curve measured at  $V_d = -1$  V).

which is a key process parameter, achieving the production of thin SnO<sub>2</sub> nanowires with an average diameter of about 40 nm. SEM investigations reveal that the average diameter as well as the length of nanowires produced was increased with an increase in the O<sub>2</sub> partial pressure. TEM and Raman analyses indicate that nanowires have a tetragonal rutile SnO<sub>2</sub> structure. Based on the XRD spectra, the FWHMs of the main SnO<sub>2</sub> peaks were increased with an increase in the O<sub>2</sub> partial pressure. We have discussed the mechanism by which the O<sub>2</sub> partial pressure affected the diameter, length, and crystallinity of nanowires. With a gate voltage varying from 10 V to -10 V, the conductance was progressively suppressed, indicating n-type semiconductor behavior.

### Acknowledgments

This work was supported by the research fund of Hanyang University (HY-2011-201100000000434).

### References

1. A. Zahoor, Q. Teng, H. Wang, M.A. Choudhry and X. Li, *Met. Mater. Int.* 17 (2011) 417-423.
2. J.Y. Park, S.-W. Choi, K. Asokan and S.S. Kim, *Met. Mater. Int.* 16 (2010) 785-788.
3. K.B. Lee, H.S. Kang and H. Kwon, *Met. Mater. Int.* 16 (2010) 799-805.
4. R. Wahab, Y.-S. Kim and H.-S. Shin, *Met. Mater. Int.* 16 (2010) 767-772.
5. S.-B. Lee, H.-Y. Lee, E. Lee, W. Lee and Y.-C. Joo, *Met. Mater. Int.* 16 (2010) 789-792.
6. H.W. Kim, M.A. Kebede, H.S. Kim, H.G. Na, J.C. Yang and C. Lee, *Mater. Int.* 16 (2010) 87-91.
7. D.Y. Lee, M.-H. Lee, N.-I. Cho, B.-Y. Kim and Y.-J. Oh, *Mater. Int.* 16 (2010) 453-457.
8. C.M. Choi, Y.C. Yoon, D.H. Hong, K.S. Brammer, K.B. Noh, Y. Oh, S.H. Oh, F.E. Talke and S.H. Jin, *Electron Mater. Lett.* 6 (2010) 59-65.
9. H.G. Moon, H.W. Jang, J.S. Kim, H.H. Park and S.J. Yoon, *Electron Mater. Lett.* 6 (2010) 27-31.
10. C.M. Choi, D.H. Hong, Y. Oh, K.B. Noh, J.Y. Kim, L. Chen, S.H. Liou and S.H. Jin, *Electron Mater. Lett.* 6 (2010) 113-117.
11. J.T. Yuh and B.S. Bae, *Electron Mater. Lett.* 6 (2010) 221-226.
12. J.H. Cho, E.J. Yoon, Y.J. Park, W.J. Ha and J.K. Kim, *Electron Mater. Lett.* 6 (2010) 51-54.
13. Y.H. Kil, M.I. Jeong, K.H. Shim, H.B. Hong, H.J. Yun, S.M. Kang, K.S. Ahn, C.J. Choi, *Electron Mater. Lett.* 6 (2010) 55-59.
14. S.G. Shin, *Electron Mater. Lett.* 6 (2010) 65-71.
15. L.A. Ma, Y. Ye, L. Q. Hu, K.L. Zheng and T.L. Guo, *Physica E* 40 (2008) 3127-3130.
16. S. Gubbala, V. Chakrapani, V. Kumar and M.K. Sunkara, *Adv. Funct. Mater.* 18 (2008) 2411-2418.
17. F. Hernandez-Ramirez, J.D. Prades, A. Tarancon, S. Barth, O. Casals, R. Jimenez-Diaz, E. Pellicer, J. Rodriguez, J.R. Morante, M.A. Juli, S. Mathur and A. Romano-Rodriguez, *Adv. Funct. Mater.* 18 (2008) 2990-2994.
18. C.H. Lin, R.S. Chen, T.T. Chen, H.Y. Chen, Y.F. Chen, K.H. Chen and L.C. Chen, *Appl. Phys. Lett.* 93 (2008) 112115:1-112115:3.
19. M.S. Saha, R.Y. Li and X.L. Sun, *Electrochem. Commun.* 9 (2007) 2229-2234.
20. S. Trohalaki, *MRS Bull.* 32 (2007) 688.
21. S. Dmitriev, Y. Lilach, B. Button, M. Moskovits and A. Kolmakov, *Nanotechnology* 18 (2007) 055707.
22. M.S. Park, G.X. Wang, Y.M. Kang, D. Wexler, S.X. Dou and H.K. Liu, *Angew. Chem. Int. Ed.* 46 (2007) 750-753.
23. O. Lupan, L. Chow, G. Chai, A. Schulte, S. Park and H. Heinrich, *Mater. Sci. Eng. B* 157 (2009) 101-104.
24. W.Y. Yin, B.Q. Wei and C.W. Hu, *Chem. Phys. Lett.* 471 (2009) 11-16.
25. Y. Wang, X. Jiang and Y. Xia, *J. Am. Chem. Soc.* 125 (2003) 16176-16177.
26. P.G. Li, M. Lei, X. Wang and W.H. Tang, *Mater. Lett.* 63 (2009) 357-359.

27. S. Thanasanvorakun, P. Mangkornong, S. Choopun and N. Mangkornong, *Ceram. Inter.* 34 (2008) 1127-1130.
28. W.Z. Wang, J.Z. Niu and L. Ao, *J. Cryst. Growth* 310 (2008) 351-355.
29. W.I. Park, Ph.D. Thesis 65 (2005).
30. Cullity B D 1978 *Elements of X-ray Diffraction* (Addison-Wesley)
31. S.H. Sun, G.W. Meng, G.X. Zhang, T. Gao, B.Y. Geng, L.D. Zhang and J. Zuo, *Chem. Phys. Lett.* 376 (2003) 103-107.
32. L. Abello, B. Bochu, A. Gaskov, S. Koudryavtseva, G. Lucazeau and M. Roumyantseva, *J. Solid State Chem.* 135 (1998) 78-85.